IMPEDANCE BOUNDARY CONDITIONS FOR ACOUSTIC WAVES IN A DUCT WITH A STEP DISCONTINUITY

DANIEL NORELAND*

Abstract. This paper treats the use of numerically computed impedance boundary conditions for acoustic simulations. Such boundary conditions may be used to combine different methods on different parts of the computational domain. Impedance boundary conditions may be computed for each subproblem independently of each other. In order to develop insight into this approach, wave propagation in a rectangular waveguide with a step discontinuity is studied.

1. Introduction. The impedance is a concept of paramount importance in acoustics [9], [7]. At the real or fictitious surface of a fluid or solid body, the impedance is defined by the relationship between the acoustic pressure $p(\omega)$ and the normal component of the particle velocity, $u_n(\omega)$. This relationship depends on the frequency ω, and it is usually non-local. It embodies a complete description of the wave response of the body to outer wave stimuli. Therefore, the impedance may be used as a boundary condition on the surface of the object, and it is possible to solve the wave problem exterior to the body without explicitly treating the interior of the body.

This study will focus on a classical example, namely a rectangular waveguide with an abrupt change in cross-sectional area. The transmission of waves in narrow tubes with abrupt changes in geometry or fluid properties has been thoroughly studied by Lighthill [9], among others. Under the assumption of longitudinal, or one-dimensional, waves, it was shown that the reflected and transmitted waves were solely determined by the mismatch of the plane wave impedance $\varrho c/S$, where ϱ, c, and S are the density of the medium, the velocity of sound, and the cross-sectional area, respectively. In this paper, we also consider transversal variations of the wave field, which are expressed by a multi-modal expansion. This leads to a generalised impedance that can be regarded as an infinite matrix that represents the transfer of energy between modes at the junction of the duct. The properties and the benefits of the impedance matrix for the numerical solution of the wave propagation problem will be illustrated.

Impedance boundary conditions (IBC:s) for domain truncation of an infinite domain have been the subject of extensive research for the last decades [16]. Methods based on Dirichlet-to-Neumann maps in boundary integral formulations or mode expansions are also applicable to finite domains with physical boundaries. The use of IBC:s makes it possible to divide the wave propagation problem into sub-problems which can be solved independently of each other. For example, consider N acoustic scatterers Ω_i, $i = 1, 2, \ldots N$, embedded in a domain Ω. The acoustical response of a scatterer Ω_i as seen from $\Omega \setminus \Omega_i$ can be

[1]Department of Information Technology, Uppsala University, Box *337*, SE-*751 05* Uppsala, Sweden.

described by an IBC according to the relation

$$Z_i u_i(\mathbf{x}) = p_i(\mathbf{x}) + f_i(\mathbf{x}),\ \mathbf{x} \in \delta\Omega_i, \tag{1}$$

where u_i and p_i are the normal velocity and the pressure at the surface of Ω_i. The impedance Z_i is an integral operator over $\delta\Omega_i$, and f_i represents sound sources within Ω_i. When the IBC(:s) (1) have been established they can be used as boundary conditions for the wave propagation problem in $\Omega - \{\Omega_i\}$, $i = 1, 2, \ldots, N$ due to the continuity of u_i and p_i at $\delta\Omega_i$, and linearity of the governing equation. This approach is particularly attractive for a number of identical scatterers at different locations, in which case only a single evaluation of the IBC is needed.

Another advantage of the approach of splitting a domain in parts and connecting the parts through the use of IBC:s, is that it is general with respect to the method for computing the boundary conditions. For instance, the IBC:s of one part of the domain may be computed using a finite-element method, another part using analytical methods, a third part using finite-differences an so on. This flexibility is advantageous eg. for long waveguides where the geometrical complexity and acoustic characteristics vary strongly [10]. The building-block technique has previously been studied by eg. Nilsson [14] and Craggs [1].

2. Physical preliminaries. In this section, the physical equations on which the argument is based are stated. Throughout this paper, it is assumed that wave propagation is linear, adiabatic and lossless. It should be pointed out, however, that only linearity is necessary for the methods presented here. A generalisation to lossy media with inhomogeneous properties does not introduce any difficulties in principle, only modifications of the governing physical equations. Forming the impedance boundary conditions can in such cases be done following the same strategy as for the simpler model examples presented here.

The acoustic pressure p of waves of the kind described above obeys the classical wave equation, which takes the form of the Helmholtz equation,

$$\Delta p + k^2 p = 0, \tag{2}$$

when a time harmonic dependence $\exp(-i\omega t)$ is assumed. The wave number k is given by $k = \omega/c$, where c is the speed of sound. The relation between the particle velocity $\mathbf{u}$, and the acoustic pressure is found from the momentum balance equation

$$i\omega\varrho\mathbf{u} = \nabla p, \tag{3}$$

where ϱ is the equilibrium density of the medium. In a bounded domain Ω, the solution to (2) is unique if appropriate boundary conditions are imposed. It is assumed that these are of Robin type, that is,

$$p - \alpha p_n = g, \qquad \text{at } \partial\Omega.$$

Here, α is a complex constant which is sometimes referred to as the *wall impedance*. The inhomogeneity term g represents an acoustic source on (part of) the boundary of the domain. For $g \equiv 0$, the equation collapses to an eigenvalue problem with solutions only for certain values of k^2.

3. The impedance concept. Consider a waveguide oriented along the $x-$axis. If the wavelength λ is much larger than the cross sectional dimensions, the waves are approximately one-dimensional [9]. The waveguide can then be described by a 2×2 *transmission matrix* relating the acoustic pressure and the volume flow velocity at the input and the output ends, respectively. This representation is valid as long as the frequency is below the cut-off frequencies of all higher transversal modes. If multi modal propagation is prevalent, a generalised transmission matrix including higher modes can be defined. Let the acoustic pressure p be expressed by the expansion

$$p(x, y, z) = \sum_n P_n(x)\varphi_n(y, z) \tag{4}$$

and the $x-$component of the particle velocity be expressed as

$$u(x, y, z) = \sum_n U_n(x)\varphi_n(y, z). \tag{5}$$

The functions φ_i need not be orthogonal, but they must constitute a system complete in L^2 in order for (4) and (5) to be valid. For e.g. cylinders and rectangular ducts, an orthogonal basis is of course directly available, but for arbitrary cross sections, a simple expression for the basis functions cannot be found. In such cases, a basis can be used consisting of the eigenfunctions of Δ_t, the tangential part of the Laplacian operator on the cross sectional area of interest.

Now, consider a waveguide segment bounded by the cross sectional areas at $x = A$ and $x = B$. Without loss of generality, it is assumed that the wall impedance α is infinite inside the waveguide, which corresponds to a sound hard wall. The waveguide segment, as part of an acoustical system, can be described by a generalised transfer matrix $\mathbf{H}$ defined through the infinite matrix relation

$$\begin{bmatrix} \mathbf{P}_A \\ \mathbf{U}_A \end{bmatrix} = \begin{bmatrix} \mathbf{H} \end{bmatrix} \begin{bmatrix} \mathbf{P}_B \\ \mathbf{U}_B \end{bmatrix}, \tag{6}$$

where the column vectors $\mathbf{P} = (P_0, P_1, \ldots)^T$ and $\mathbf{U} = (U_0, U_1, \ldots)^T$ contain the expansion coefficients defined by (4) and (5) evaluated at $x = A$ and $x = B$. All information regarding the behaviour of the segment is contained in $\mathbf{H}$. Thus, knowing the transfer matrix, the solution of (2) in the domain $\Omega \setminus \Omega_{AB}$ can be uniquely calculated, without the explicit treatment of the interior of Ω_{AB}. An application where the use of transfer matrices is useful, is the analysis of chain-like structures consisting of several duct segments. After forming the transfer

matrix of each individual segment, the transfer matrix of the whole structure is obtained as the matrix product of the respective segments. This approach is, of course, particularly well suited for cases where a waveguide configuration is analysed repeatedly, with only local changes of the geometry.

Although (6) is generally valid in principle, transfer matrices are often useless from a numerical point of view.[1] The elements of $\mathbf{H}$ corresponding to evanescent modes grow exponentially with the length of the segment. The exponential growth is stronger, the higher the number of the mode. Thus, the computation of transfer matrices is an ill-posed problem.

The problem with $\mathbf{H}$ getting singular can be overcome by instead working with a generalised impedance matrix, defined by

$$\begin{bmatrix} \mathbf{P}_A \\ \mathbf{P}_B \end{bmatrix} = \begin{bmatrix} \mathbf{Z} \end{bmatrix} \begin{bmatrix} \mathbf{U}_A \\ \mathbf{U}_B \end{bmatrix}. \tag{7}$$

Before proceeding, let us make a short digression on how the impedance matrix formulation differs from the tranmission matrix formulation. From (6) it is observed that the pressure or velocity at A is expressed only as a function of the conditions at B. Therefore, as the interfaces at A and B become acoustically decoupled from each other, either due to the presence of exponentially decaying evanescent modes, or due to visco-thermal losses in the waveguide, the elements of $\mathbf{H}$ tend to infinity. The formulation (7), on the other hand, does not have this property. A block matrix formulation of equation (7),

$$\mathbf{Z} = \left[\begin{array}{c|c} \mathbf{Z}_{11} & \mathbf{Z}_{12} \\ \hline \mathbf{Z}_{21} & \mathbf{Z}_{22} \end{array}\right],$$

indicates that decoupling of the end interfaces appears as the off-diagonal blocks $\mathbf{Z}_{12}$ and $\mathbf{Z}_{21}$ having small elements as compared to $\mathbf{Z}_{11}$ and $\mathbf{Z}_{22}$. Also the impedance matrix may be singular. It should be noted, however, that this singularity is of a different nature than the singularity of $\mathbf{H}$, and it rarely poses any practical problems. A trivial example of such an occasion is the impedance of an ideal open-end termination, that is $p = 0$ at the end surface.

The relation between $\mathbf{H}$ and $\mathbf{Z}$ is deduced from a block matrix formulation of Eq. (6),

$$\begin{bmatrix} \mathbf{P}_A \\ \mathbf{U}_A \end{bmatrix} = \left[\begin{array}{c|c} \mathbf{H}_{11} & \mathbf{H}_{12} \\ \hline \mathbf{H}_{21} & \mathbf{H}_{22} \end{array}\right] \begin{bmatrix} \mathbf{P}_B \\ \mathbf{U}_B \end{bmatrix}. \tag{8}$$

Rewriting this equations yields

$$\begin{bmatrix} \mathbf{P}_A \\ \mathbf{P}_B \end{bmatrix} = \left[\begin{array}{c|c} \mathbf{H}_{11}\mathbf{H}_{21}^{-1} & \mathbf{H}_{12} - \mathbf{H}_{11}\mathbf{H}_{21}^{-1}\mathbf{H}_{22} \\ \hline \mathbf{H}_{21}^{-1} & -\mathbf{H}_{21}^{-1}\mathbf{H}_{22} \end{array}\right] \begin{bmatrix} \mathbf{U}_A \\ \mathbf{U}_B \end{bmatrix}. \tag{9}$$

[1] One of few applications where transfer matrices are frequently used is in the analysis of narrow waveguides where wave propagation can be considered as one-dimensional. If there are losses in the system, also the propagating mode undergoes a slow exponential decay with distance. This is usually less of a problem than evanescent modes, at least for short waveguides.

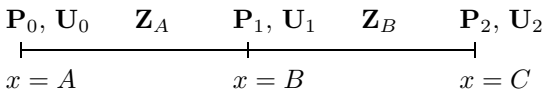

FIG. 1. *Schematic picture of two waveguides connected in series.*

Notice that the transformation from $\mathbf{Z}$ to $\mathbf{H}$ has the same form as the transformation from $\mathbf{H}$ to $\mathbf{Z}$. We have

$$\left[\begin{array}{c} \mathbf{P}_A \\ \mathbf{U}_A \end{array}\right] = \left[\begin{array}{c|c} \mathbf{Z}_{11}\mathbf{Z}_{21}^{-1} & \mathbf{Z}_{12} - \mathbf{Z}_{11}\mathbf{Z}_{21}^{-1}\mathbf{Z}_{22} \\ \hline \mathbf{Z}_{21}^{-1} & -\mathbf{Z}_{21}^{-1}\mathbf{Z}_{22} \end{array}\right] \left[\begin{array}{c} \mathbf{P}_B \\ \mathbf{U}_B \end{array}\right].$$

A single impedance matrix for a series of adjacent sections may be formed by a proper combination of local impedances. Figure 1 shows two waveguides attached in series with each other. The impedance matrices of the two waveguides are denoted $\mathbf{Z}_A$ and $\mathbf{Z}_B$, respectively. The impedance matrix $\mathbf{Z}_{AB}$ of the two waveguides together is found by eliminating $\mathbf{U}_1$ from the identities

$$\mathbf{P}_0 = \mathbf{Z}_{A11}\,\mathbf{U}_0 + \mathbf{Z}_{A12}\,\mathbf{U}_1 \tag{10a}$$
$$\mathbf{P}_2 = \mathbf{Z}_{B21}\,\mathbf{U}_1 + \mathbf{Z}_{B22}\,\mathbf{U}_2. \tag{10b}$$

Since the pressure $\mathbf{P}_1$ and the velocity $\mathbf{U}_1$ must be continuous across the interface at $x = B$, they can be expressed in terms of $\mathbf{U}_0$ and $\mathbf{U}_2$ using

$$\mathbf{P}_1 = \mathbf{Z}_{B11}\,\mathbf{U}_1 + \mathbf{Z}_{B12}\,\mathbf{U}_2, \tag{11a}$$
$$\mathbf{P}_1 = \mathbf{Z}_{A21}\,\mathbf{U}_0 + \mathbf{Z}_{A22}\,\mathbf{U}_1. \tag{11b}$$

These relations are used for the elimination of $\mathbf{U}_1$ from Eq. (10). This yields

$$\left[\begin{array}{c} \mathbf{P}_0 \\ \mathbf{P}_2 \end{array}\right] = \left[\begin{array}{cc} \mathbf{Z}_{AB11} & \mathbf{Z}_{AB12} \\ \mathbf{Z}_{AB21} & \mathbf{Z}_{AB22} \end{array}\right] \left[\begin{array}{c} \mathbf{U}_0 \\ \mathbf{U}_2 \end{array}\right], \tag{12}$$

where

$$\begin{aligned}
\mathbf{Z}_{AB11} &= \mathbf{Z}_{A11} + \mathbf{Z}_{A12}(\mathbf{Z}_{B11} - \mathbf{Z}_{A22})^{-1}\mathbf{Z}_{A21}, \\
\mathbf{Z}_{AB12} &= -\mathbf{Z}_{A12}(\mathbf{Z}_{B11} - \mathbf{Z}_{A22})^{-1}\mathbf{Z}_{B12}, \\
\mathbf{Z}_{AB21} &= \mathbf{Z}_{B21}(\mathbf{Z}_{B11} - \mathbf{Z}_{A22})^{-1}\mathbf{Z}_{A21}, \\
\mathbf{Z}_{AB22} &= \mathbf{Z}_{B22} - \mathbf{Z}_{B21}(\mathbf{Z}_{B11} - \mathbf{Z}_{A22})^{-1}\mathbf{Z}_{B12}.
\end{aligned}$$

Next, assume that the waveguide in Fig. 1 is terminated by the boundary conditions

$$\mathbf{P}_L = \mathbf{Z}_L \mathbf{U}_L + \mathbf{F}_L \quad \text{at } x = A \tag{13}$$

$$\mathbf{P}_R = \mathbf{Z}_R \mathbf{U}_R + \mathbf{F}_R \quad \text{at } x = C \tag{14}$$

where $\mathbf{Z}_L$ and $\mathbf{Z}_R$ are the load impedances, and the terms $\mathbf{F}_L$ and $\mathbf{F}_R$ represent the sources outside the domain $[A, C]$. Using the continuity conditions

$$\mathbf{P}_0 = \mathbf{P}_L, \mathbf{U}_0 = \mathbf{U}_L, \quad \text{at } x = A \tag{15}$$

$$\mathbf{P}_2 = \mathbf{P}_R, \mathbf{U}_2 = \mathbf{U}_R, \quad \text{at } x = C \tag{16}$$

$$\tag{17}$$

we obtain the system

$$\begin{bmatrix} \mathbf{Z}_{AB11} & \mathbf{Z}_{AB12} \\ \mathbf{Z}_{AB21} & \mathbf{Z}_{AB22} \end{bmatrix} \begin{bmatrix} \mathbf{U}_0 \\ \mathbf{U}_2 \end{bmatrix} = \begin{bmatrix} \mathbf{Z}_L \mathbf{U}_0 + \mathbf{F}_L \\ \mathbf{Z}_R \mathbf{U}_2 + \mathbf{F}_R \end{bmatrix}, \tag{18}$$

for the velocities at the endpoints. One could equally well set up equations for the pressures at the endpoints.

There are two major tasks in pursuing this approach. First, the impedance of each section must to be computed. This can be done by applying wave propagation solvers. After that, all IBC:s are assembled to set up equations for the pressure (or velocity) at the interfaces. Once these are known, the wave propagation solvers are re-invoked to compute the pressure field within each section.

Apparently, the prize for the numerical convenience of working with impedance matrices is an increase in the computational work when analysing chain structures. The special case of a large number N of equal waveguide segments connected in series has been treated in a paper by Craggs [1], where the segments are lumped in groups whose lengths are doubled recursively. Using this simple arrangement, the condensed impedance matrix can be computed in $\log N$ operations of the type (12). For an arbitrary series of waveguides however, it is difficult to reduce the work, apart from making proper use of factorisations of the matrices that are formally inverted in (12). This is a topic of future research.

4. Near and far field properties of impedance boundary conditions. A feature shared by many duct acoustic problems is the distinction between acoustic near- and far fields. A common, rather loose, definition of the near field around a sound source or scatterer is the region of space within a distance of a fraction of a wavelength from the source. Since all modes above the cut-off frequency are evanescent, these components of the wave field are negligible sufficiently far away from the place where they originated, that is, where they were actively generated or excited through modal conversion. For a channel, it is therefore natural to define the distinction between near and far field as

the portion of the wave field belonging to the evanescent modes. In the extreme vicinity of a scatterer, it is relevant to instead distinguish between acoustic mono poles, dipoles and so on.

If an impedance boundary condition is placed in the vicinity of a region where modal conversion takes place, that is where acoustic energy is redistributed between different modes, one can expect a strong degree of coupling between a number of modes. This coupling shows up as large coefficients in the transfer and impedance matrices. As the modal number increases, the corresponding wave numbers attain larger imaginary parts, and thus become increasingly quickly evanescent. The weaker interaction between two higher order modes, or a lower and a higher order mode is manifested through small corresponding coefficients in the impedance matrix. The elements along the diagonal of an impedance matrix decay slower, however, since these elements are associated to the self-coupling between modes and their respective normal derivatives.

The magnitudes of the elements can be expected to depend strongly on the location of the impedance boundary condition. Placed near a region of strong modal coupling, the impedance matrix can be expected to have a larger number of elements of relatively large magnitude, than if the boundary is located further away. In the far field limit, only a few coefficients will be significantly different from zero.

5. Numerical examples. This section presents examples of how impedance boundary conditions can be formed and used in a practical case. The application is to represent a channel with a step discontinuity by an IBC. Although the stepped channel problem is one example of many possible, it has – and still continues to – attract interest in its own right (cf. [6] and [12]). Some time is devoted to the specific problem *per se*.

Figure 2 shows the model problem for which a numerical impedance boundary condition was calculated. The geometry of the problem is a two dimensional planar channel that extends to infinity in the positive and the negative $x-$direction. The channel has a step discontinuity at $x = 0$. If planar waves are assumed to be generated at $x = -\infty$, a reflection–transmission process will take place at the discontinuity. In the process, acoustic energy is redistributed between different modes. The modal pattern is complicated near the discontinuity, but as the distance increases, evanescent modes decay and only propagating modes are prevalent.

The aim of this section is to present an experiment where the part of the waveguide for which $x > L$, $L < 0$ is represented by an impedance boundary condition. It is assumed that this system is acoustically passive, i.e no left travelling waves exist at $x > 0$. In order to simplify notation, the impedance boundary condition is defined through the relation

$$\mathbf{P}_L = \mathbf{Z}_L \frac{\partial}{\partial x} \mathbf{P}_L. \tag{19}$$

Equation (19) is equivalent to Eq. (1) for $f_i = 0$, with the exception that the

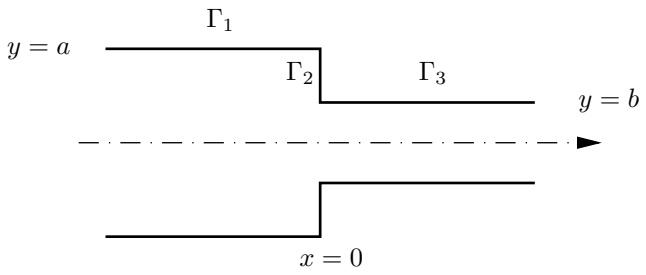

FIG. 2. *A test geometry.*

physical constants entering through Eq. (3) are omitted.

5.1. The continuous case. Here we consider the construction of an impedance boundary condition representing the geometry with a stepped channel, truncated at $x = L < 0$.

5.1.1. Continuous solution to the Helmholtz equation using mode matching. The solution to the Helmholtz equation

$$\begin{cases} \Delta p + k^2 p = 0 \\ \quad \partial p/\partial n = 0 \qquad \text{on } \Gamma_1 \cup \Gamma_2 \cup \Gamma_3, \end{cases} \tag{20}$$

on the geometry of Fig. 2 can be expressed as an infinite expansion of planar channel modes. Considering for simplicity only modes symmetric with respect to $y = 0$, and setting $c = 1$, the solution to (20) for $x \leq 0$ can be written as

$$p_l(x, y) = \sum_{n=0}^{\infty} \cos\left(\frac{n\pi y}{a}\right) \left(A_n e^{ik_l^{(n)} x} + B_n e^{-ik_l^{(n)} x}\right), \tag{21}$$

a solution that satisfies the boundary condition on Γ_1. Here,

$$k_l^{(n)} = \sqrt{\omega^2 - \frac{n^2\pi^2}{a^2}}, \quad \mathrm{Im}(k_l^{(n)}) \geq 0$$

are the longitudinal wave numbers. For a time dependence $\exp(-i\omega t)$, the A_n:s are the complex amplitudes of waves travelling to the right. Modes for which $k_n = i\alpha$, $\alpha > 0$, are evanescent in the sense that they exhibit an exponential decay along the direction of propagation. The frequency ω_{cn} for which $k_l^{(n)} = 0$ is called the *cut-off* frequency for mode n, and is given by

$$\omega_{cn} = n\pi/a. \tag{22}$$

In the same way as for $x \leq 0$,

$$p_r(x, y) = \sum_{n=0}^{\infty} \cos\left(\frac{n\pi y}{b}\right) \left(C_n e^{ik_r^{(n)} x} + D_n e^{-ik_r^{(n)} x}\right), \quad x > 0 \tag{23}$$

where

$$k_r^{(n)} = \sqrt{\omega^2 - \frac{n^2\pi^2}{b^2}}.$$

Since no waves are generated at $x \to \infty$, $D_n = 0\ \forall n$. For any right travelling wave

$$\mathbf{A} = (A_0, A_1, A_2, \ldots)^T, \qquad k = 0, 1, \ldots$$

the generalised reflection and transmission coefficients

$$\mathbf{B} = (B_0, B_1, B_2, \ldots)^T, \qquad k = 0, 1, \ldots$$

and

$$\mathbf{C} = (C_0, C_1, C_2, \ldots)^T, \qquad k = 0, 1, \ldots$$

are chosen such that the boundary condition on Γ_2 is satisfied, as well as the physical matching conditions that both p and $\partial p/\partial x$ are continuous at $x = 0$, $-b \leq y \leq b$,

$$p_l(0, y) = p_r(0, y), \quad -b \leq y \leq b, \tag{24a}$$

$$\frac{\partial p_l(0, y)}{\partial x} = \frac{\partial p_r(0, y)}{\partial x}, \quad -b \leq y \leq b. \tag{24b}$$

In practice, the sums of the expansions have to be truncated in order to solve the resulting system of equations. However, after this truncation it is no longer possible to satisfy Eq. (24) and the boundary condition on Γ_2. Instead, a weak formulation of (24) can be stated; Using N modes for p_l and M modes for p_r, the weak formulation of the continuity conditions at $x = 0$ is obtained by multiplying the expansions (21) and (23) with the expansion basis functions, and integrating over the appropriate intervals. For Eq. (24a) it is natural to choose the basis functions from (23), and integrate over the interval $-b \leq y \leq b$.

$$\sum_{n=0}^{N-1} A_n \int_{-b}^{b} \cos\left(\frac{n\pi y}{a}\right) \cos\left(\frac{m\pi y}{b}\right) dy + \sum_{n=0}^{N-1} B_n \int_{-b}^{b} \cos\left(\frac{n\pi y}{a}\right) \cos\left(\frac{m\pi y}{b}\right) dy = \\ = \sum_{n=0}^{M-1} C_n \int_{-b}^{b} \cos\left(\frac{n\pi y}{b}\right) \cos\left(\frac{m\pi y}{b}\right) dy, \qquad m = 0, 1, \ldots, M-1. \tag{25}$$

In the same way,

$$\begin{aligned}
&\sum_{n=0}^{N-1} ik_l^{(n)} A_n \int_{-a}^{a} \cos\Big(\frac{n\pi y}{a}\Big)\cos\Big(\frac{m\pi y}{a}\Big)\,dy + \\
&-\sum_{n=0}^{N-1} ik_l^{(n)} B_n \int_{-a}^{a} \cos\Big(\frac{n\pi y}{a}\Big)\cos\Big(\frac{m\pi y}{a}\Big)\,dy = \\
&=\sum_{n=0}^{M-1} ik_r^{(n)} C_n \int_{-b}^{b} \cos\Big(\frac{n\pi y}{b}\Big)\cos\Big(\frac{m\pi y}{a}\Big)\,dy, \qquad m=0,1,\ldots,N-1.
\end{aligned} \tag{26}$$

Equation (26) corresponds to the flow balance equation along $x = 0$, although only the planar mode has a net flow contribution. The boundary condition at Γ_2 is implicitly imposed in that the integration interval of the left hand side of (26) is extended to $-a \le y \le a$. This can be done since $\partial p_l/\partial x = 0$ on $-a \le y \le -b$ and $b \le y \le a$.

For each m, Eq. (25) and (26) form one row of a linear system of equations in $\mathbf{B}$ and $\mathbf{C}$. After rearranging terms, this system can be written in block form as

$$\begin{bmatrix} \mathbf{W}^1_{M\times N} & \mathbf{W}^2_{M\times M} \\ \mathbf{W}^3_{N\times N} & \mathbf{W}^4_{N\times M} \end{bmatrix} \begin{bmatrix} \mathbf{B} \\ \mathbf{C} \end{bmatrix} = \begin{bmatrix} \mathbf{Q}^1_{M\times N} \\ \mathbf{Q}^2_{N\times N} \end{bmatrix} \mathbf{A}, \tag{27}$$

or more compactly

$$\mathbf{W}\begin{bmatrix} \mathbf{B} \\ \mathbf{C} \end{bmatrix} = \mathbf{Q}\mathbf{A} \tag{28}$$

where

$$\begin{aligned}
Q^1_{mn} &= \int_{-b}^{b} \cos\left(\frac{(n-1)\pi y}{a}\right)\cos\left(\frac{(m-1)\pi y}{b}\right)\,\mathrm{d}y, \\
Q^2_{mn} &= -\int_{-b}^{b} \cos\left(\frac{(n-1)\pi y}{b}\right)\cos\left(\frac{(m-1)\pi y}{b}\right)\,\mathrm{d}y, \\
Q^3_{mn} &= -i\sqrt{\omega^2 - \frac{(n-1)^2\pi^2}{a^2}}\int_{-a}^{a} \cos\left(\frac{(n-1)\pi y}{a}\right)\cos\left(\frac{(m-1)\pi y}{a}\right)\mathrm{d}y, \\
Q^4_{mn} &= -i\sqrt{\omega^2 - \frac{(n-1)^2\pi^2}{b^2}}\int_{-b}^{b} \cos\left(\frac{(n-1)\pi y}{b}\right)\cos\left(\frac{(m-1)\pi y}{a}\right)\mathrm{d}y,
\end{aligned}$$

and

$$\mathbf{Q}^1 = -\mathbf{W}^1, \quad \mathbf{Q}^2 = \mathbf{W}^3\,.$$

The integrals of these expressions are expanded using the identities

$$\int_{-b}^{b} \cos\left(\frac{n\pi y}{a}\right) \cos\left(\frac{m\pi y}{b}\right) \mathrm{d}y =$$
$$\begin{cases} \frac{\sin(\frac{n\pi y}{a} - \frac{m\pi y}{b})}{\frac{n\pi}{a} - \frac{m\pi}{b}} + \frac{\sin(\frac{n\pi y}{a} + \frac{m\pi y}{b})}{\frac{n\pi}{a} + \frac{m\pi}{b}} & \left(\frac{n\pi}{a}\right)^2 \neq \left(\frac{m\pi}{b}\right)^2, \\ b & \left(\frac{n\pi}{a}\right)^2 = \left(\frac{m\pi}{b}\right)^2, \quad n, m \neq 0, \\ 2b & n = m = 0, \end{cases}$$

and

$$\int_{-b}^{b} \cos\left(\frac{n\pi y}{b}\right) \cos\left(\frac{m\pi y}{b}\right) \mathrm{d}y = \begin{cases} 0, & n \neq m, \\ b, & n = m \neq 0, \\ 2b, & n = m = 0. \end{cases}$$

Through orthogonality, $\mathbf{W}^2$ and $\mathbf{W}^3$ of Eq. (27) are diagonal, but $\mathbf{W}^1$ and $\mathbf{W}^4$ are dense.

In many applications, such as in musical instruments, cylindrical waveguides are used. The solution of the Helmholtz equation around a step discontinuity in a cylindrical geometry can be carried out along the same lines as in the present section (see Appendix A).

5.1.2. A convergence study. The accuracy of the mode matching solution depends not only on the modal resolution, but also on ratio between N and M. It has been found that N/M must equal the ratio between the characteristic dimensions of the waveguide to the left and to the right of the discontinuity for the solution to converge to the right value. This phenomenon, known as the problem of *relative convergence*, has been studied theoretically for the iris discontinuity problem in electromagnetics by Mittra et al. [11]. Muehleisen and Swanson [13] have investigated the problem numerically for acoustic waveguides with a step discontinuity. In the problem with a stepped channel, the correct choice of M is given by $N/M = a/b$. Corresponding three-dimensional relations exist for junctions between e.g. two rectangular waveguides, but for more general discontinuities, a simple a-priori expression for the correct choice of resolution does not seem to exist. Intuitively, it seems reasonable to resolve the regions $x < 0$ and $x > 0$ equally well by letting the highest transversal wavenumber in the two regions correspond to equally rapid spatial variations of the solution. What is less intuitive, is that an increase of the resolution in one of the regions can in fact decrease the overall accuracy of the solution.

An interesting question is what the rate of convergence is as N increases, and whether the problem of relative convergence is prevalent also here. It is beyond the scoop of this paper to carry out an in-depth investigation of these matters, but a numerical study is presented in this section.

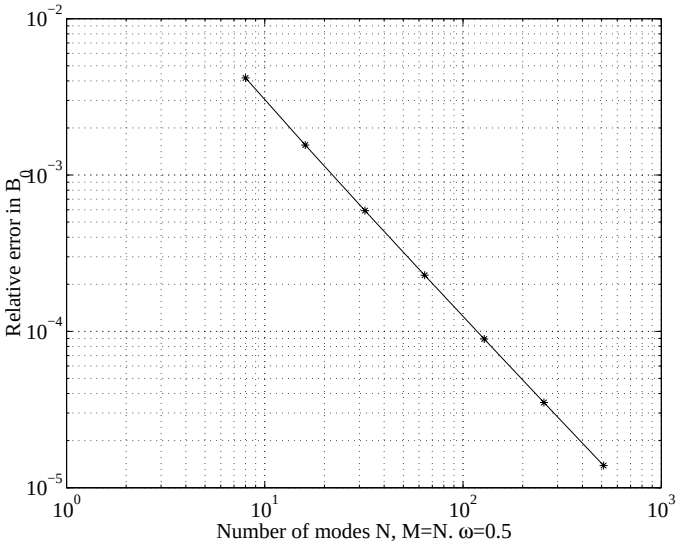

FIG. 3. *Relative error in B_0 as a function of N. $M = N$, $\omega = 0.5$.*

An experiment was made, in which the errors in the computed coefficients of $\mathbf{B}$ were studied as a function of N for an incoming wave $A_n = \delta_{0n}$. The geometry of the channel was that shown in figure 2, with $a = 3$ and $b = 3/2$. The cut-off frequencies of B_1 and B_2 for this problem are $w_{c1} = 1.0472$ and $w_{c2} = 2.0944$. As a reference value, a solution (further commented below) computed with a high number of modes was used. Figure 3 and 4 show the relative error in B_0 computed with $M = N$ and $M = Nb/a$, respectively. The frequency, $\omega = 0.5$, is about half of the cut-off frequency of B_1. Thus, B_0 is the only propagating mode in this experiment.

The first observation is that the problem of relative convergence seems to be absent, at least as far as it was possible to chose the modal resolution here. This seems at first to contradict the results by Mittra et al. [11], but the formulation of their mode-matching equation is slightly different from the formulation in the present paper.

The nearly linear curves in the log-log diagrammes indicate a dependence of the type $\epsilon \approx N^{-p}$ for both ways of selecting M. Importantly however, the error decreases quicker for $M = Nb/a$ that for $M = N$, although a smaller number of modes is used in the former case.

In order to investigate the convergence more closely, the *control quotient*

$$r = \frac{B(N) - B(2N)}{B(2N) - B(4N)}$$

for B_0 and B_1 was calculated for some different choices of N. If $B(N)$ is an

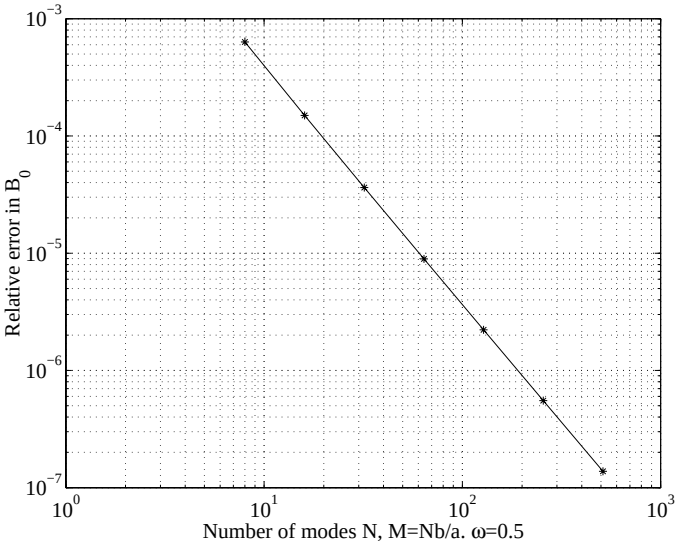

FIG. 4. *Relative error in B_0 as a function of N. $M = Nb/a$, $\omega = 0.5$.*

			$\log_2(r)$	
N	$2N$	$4N$	$M = N$	$M = Nb/a$
64	128	256	$1.3628 + 0.0001i$	$2.0130 - 0.0000i$
128	256	512	$1.3510 + 0.0001i$	$2.0065 - 0.0000i$
256	512	1024	$1.3439 + 0.0000i$	$2.0033 - 0.0000i$
512	1024	2048	$1.3396 + 0.0000i$	$2.0016 + 0.0000i$

TABLE 1
Control quotients for B_0. $\omega = 0.5$.

approximation of B of order $\mathcal{O}(N^{-p})$, then

$$\lim_{N\to\infty} \frac{B(N) - B(2N)}{B(2N) - B(4N)} = 2^p \,.$$

Table 1 and 2 show control quotients for the experiment with $\omega = 0.5$. The convergence was also studied for a frequency with several propagating modes. Table 3 and 4 show the convergence rate for the case $\omega = 2.2$, which is slightly above the cut-off frequency of B_2.

For the incorrect choice of N/M, the convergence rate is like $N^{-4/3}$. Experiments with other choices of M, e.g. $M = 3Nb/(4a)$, support this assumption. When $M = Nb/a$, the figures of the tables give a strong indication that the method is of order $\mathcal{O}(N^{-2})$. As Tables 1–4, show the rate is the same for B_0 and B_1, and is independent of the frequency ω.

			$\log_2(r)$	
N	$2N$	$4N$	$M = N$	$M = Nb/a$
64	128	256	$1.3378 - 0.0066i$	$2.0132 + 0.0000i$
128	256	512	$1.3350 - 0.0042i$	$2.0066 + 0.0000i$
256	512	1024	$1.3337 - 0.0027i$	$2.0033 + 0.0000i$
512	1024	2048	$1.3331 - 0.0017i$	$2.0016 + 0.0000i$

TABLE 2
Control quotients for B_1. $\omega = 0.5$.

			$\log_2(r)$	
N	$2N$	$4N$	$M = N$	$M = Nb/a$
64	128	256	$1.3902 + 0.0347i$	$2.0132 - 0.0003i$
128	256	512	$1.3687 + 0.0225i$	$2.0066 - 0.0001i$
256	512	1024	$1.3552 + 0.0144i$	$2.0033 - 0.0000i$
512	1024	2048	$1.3467 + 0.0091i$	$2.0016 - 0.0000i$

TABLE 3
Control quotients for B_0. $\omega = 2.2$.

In order to further investigate the convergence properties, Romberg's extrapolation method was applied to approximations for B_0 computed for $N = 8, 16, 32, \ldots, 2048$ and the correct choice of M. A study of the control quotients for the obtained values shows that each extrapolation step increases the order of accuracy by one, as long as is allowed by the avaliable floating point precision.[2] The reference value used for Fig. 3 and 4 was computed in this way, and has about 14 correct figures. When Romberg extrapolation was applied for values obtained with an incorrect choice of M, it was not possible to detect any consistent algebraic order of accuracy after the $\mathcal{O}(N^{-3/4})$ had been cancelled.

It should be noted that we are applying a spectral method with an exponential rate of convergence for smooth solutions [3]. In the present example the solution possesses less regularity around the corner, and this can be expected to diminish the convergence rate of the solution (cf. Johnsson [5]). In the vicinity of a corner of opening angle $\gamma = 3\pi/2$, the solution of the Helmholtz equation is of the form

$$p(r, \theta) = r^{2/3} f_1(\theta) + f_2(r, \theta), \tag{29}$$

an expression whose gradient is singular at the corner $r = 0$. The form of the solution can be shown quite simply by solving the Helmholtz equation

$$\begin{cases} \Delta p + k^2 p = 0, \\ \quad \partial p / \partial \theta = 0, \quad \theta = 0, 3\pi/2 \end{cases}$$

[2]In none of the investigated cases did the convergence break down before order five, and for some cases, convergence up to order eight was detected.

			$\log_2(r)$	
N	$2N$	$4N$	$M = N$	$M = Nb/a$
64	128	256	$1.3540 - 0.0283i$	$2.0128 + 0.0001i$
128	256	512	$1.3449 - 0.0171i$	$2.0065 + 0.0000i$
256	512	1024	$1.3397 - 0.0105i$	$2.0033 + 0.0000i$
512	1024	2048	$1.3369 - 0.0065i$	$2.0016 + 0.0000i$

TABLE 4
Control quotients for B_1. $\omega = 2.2$.

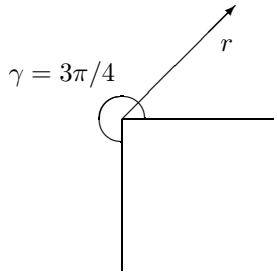

FIG. 5. *An exterior corner.*

on the geometry defined by Fig. 5. Using the method of separation of variables, the solutions are found to be of the form

$$p_m(r,\theta) = J_m(kr)\cos(m\theta), \quad m = 0, \frac{2}{3}, \frac{4}{3}, \ldots,$$

where k is a radial wave number. In the model of the corner, no outer boundary was specified, whence k is arbitrary. The fact that θ runs from 0 to $3\pi/2$, instead of the more familiar 0 to 2π, is reflected by the property that the Bessel functions J_m are of fractional order. By series expansion, it is found that

$$J_0(kr) = 1 - \frac{k^2r^2}{4} + \frac{k^4r^4}{64} + \mathcal{O}(r^6)$$

$$J_{2/3}(kr) = \frac{3}{4}\,\frac{\sqrt[3]{2}k^{2/3}r^{2/3}}{\Gamma(2/3)} - \frac{9}{80}\,\frac{\sqrt[3]{2}k^{8/3}r^{8/3}}{\Gamma(2/3)} + \frac{27}{5120}\,\frac{\sqrt[3]{2}k^{14/3}r^{14/3}}{\Gamma(2/3)} + \mathcal{O}(r^6)$$

$$J_{4/3}(kr) = \frac{9}{32}\,\frac{2^{2/3}k^{4/3}\sqrt{3}\Gamma(2/3)r^{4/3}}{\pi} - \frac{27}{896}\,\frac{2^{2/3}k^{10/3}\sqrt{3}\Gamma(2/3)r^{10/3}}{\pi} + \mathcal{O}(r^6)$$

Apparently, it is only the first expansion term of $J_{2/3}$ that poses a problem at $r = 0$, and we see that (29) holds with f_2 differentiable at $r = 0$.

In acoustics, the complicated near field of a source or scatterer is usually of little interest. The far field, though, is of great importance. In the present example, the far field is represented by the back reflected modes with real wave numbers $k_l^{(n)}$. The numerical results in Tables 1– 4 show that the use of a high-order method in general has little impact on the rate of convergence. However,

	10^{-6}	0.5	1
B_0	0.2500 - 0.0000i	$0.2573 - 0.0735i$	$0.3638 - 0.2691i$
B_1	-0.0000 + 0.0000i	$-0.0341 + 0.3443i$	$-0.5503 + 1.3011i$
B_2	0.0000 - 0.0000i	$0.0090 - 0.0907i$	$0.1165 - 0.2754i$
B_3	0.0000 - 0.0000i	$0.0013 - 0.0128i$	$0.0034 - 0.0080i$
B_4	-0.0000 + 0.0000i	$-0.0032 + 0.0319i$	$-0.0339 + 0.0802i$
	1.5	2	2.5
B_0	$0.4188 - 0.0281i$	$0.4123 - 0.0463i$	$0.3956 - 0.0137i$
B_1	$-0.8480 + 0.0777i$	$-0.7024 + 0.0568i$	$-0.6622 + 0.0080i$
B_2	$0.1198 - 0.1306i$	$0.4596 - 0.4646i$	$0.3526 + 0.0332i$
B_3	$-0.0196 - 0.0441i$	$-0.0210 - 0.0538i$	$-0.0441 - 0.1496i$
B_4	$-0.0267 + 0.0500i$	$-0.0432 + 0.0798i$	$-0.0170 + 0.1087i$

TABLE 5

Reflection coefficients for different modal numbers and frequencies. A convergence study certifies the correctness of the presented figures. $\omega = 10^{-6}$ is an approximation of the low-frequency limit $\omega = 0$, for which Eq. (28) becomes singular. (For $\omega = 10^{-6}$, $\mathrm{cond}(\mathbf{W}) \approx 6 \cdot 10^7$.)

by carefully selecting the number of modes in the truncated sums, it is possible to obtain approximations of the coefficients in $\mathbf{B}$ with an error expansion of the form

$$\epsilon = c_2 N^{-2} + c_3 N^{-3} + c_4 N^{-4} + \dots$$

Apart from this, the only way to improve accuracy of the far-field solution is to refine the spatial resolution around the corner. One way to accomplish this, when utilising methods based on a spatial discretisation, is to use adaptive grids as in the finite-element method [2]. As an alternative, the following approach is suggested; In a strip around $x = 0$ a very fine discretisation is employed. At the fictitious interface $x = x_L$, $x_L < 0$, a coarse discretisation for $x < x_L$ is connected to the fine one by the use of IBC:s.

5.1.3. Comparison to the one-dimensional approximation. The first five coefficients of $\mathbf{B}$, computed for different values of ω in a geometry $a = 3$ and $b = 9/5$ are shown in table 5[3]. The values of the first row should be compared to the one-dimensional approximation of the reflection coefficients at an impedance discontinuity. The reflection coefficient of an interface between two waveguides of characteristic impedance Z_l and Z_r is given by

$$R = \frac{Z_r - Z_l}{Z_r + Z_l}. \tag{30}$$

[3]The somewhat strange relation between a and b is motivated by the discretisation in section 5.2, for which this choice makes it convenient to refine the discretisation.

The characteristic impedance Z of a waveguide of cross-sectional area S is, in turn, given by $Z = \varrho c/S$. In the present example, Eq. (30) yields a reflection coefficient of $1/4$. As expected, the one-dimensional approximation is good for low frequencies, but fails completely at $\omega = 1$ – near the cut-off frequency of B_1. Here, this mode is strongly activated. At $\omega = 2$, which is close to the cut-off frequency of B_2, also that mode becomes excited. Note, however, that the fact that the coefficients of evanescent modes may be large, and in some cases exceed one, does not violate the energy flow balance. Evanescent modes store acoustic energy, but do not propagate it.

5.1.4. Computing the impedance matrix. From the equations

$$p(L,y) = \sum_{n=0}^{N} A_n e^{ik_l^{(n)}L} \cos\left(\frac{n\pi y}{a}\right) + \sum_{n=0}^{N} B_n e^{-ik_l^{(n)}L} \cos\left(\frac{n\pi y}{a}\right), \tag{31a}$$

$$p_x(L,y) = \sum_{n=0}^{N} A_n ik_l^{(n)} e^{ik_l^{(n)}L} \cos\left(\frac{n\pi y}{a}\right) - \sum_{n=0}^{N} B_n ik_l^{(n)} e^{-ik_l^{(n)}L} \cos\left(\frac{n\pi y}{a}\right) \tag{31b}$$

and (19), we have

$$\mathbf{D}_1\mathbf{A} + \mathbf{D}_2\mathbf{B} = \mathbf{Z}_L\left(\mathbf{D}_3\mathbf{A} + \mathbf{D}_4\mathbf{B}\right) \tag{32}$$

where

$$\mathbf{D}_1 = \mathbf{\Lambda}\left(e^{ik_l^{(n)}L}\right), \qquad \mathbf{D}_2 = \mathbf{\Lambda}\left(e^{-ik_l^{(n)}L}\right),$$
$$\mathbf{D}_3 = \mathbf{\Lambda}\left(ik_l^{(n)}e^{ik_l^{(n)}L}\right), \quad \mathbf{D}_4 = \mathbf{\Lambda}\left(-ik_l^{(n)}e^{-ik_l^{(n)}L}\right).$$

Here, $\mathbf{\Lambda}(d(n))$ denotes a diagonal matrix with $d(0), d(1), \ldots$ on the diagonal. From Eq. (28), we have that

$$\mathbf{B} = \mathbf{T}\mathbf{W}^{-1}\mathbf{Q}\mathbf{A}, \tag{33}$$

where $\mathbf{T}$ is an N by $N+M$ observation matrix given by

$$T_{ij} = \begin{cases} 1, & i = j \\ 0, & i \neq j\,. \end{cases}$$

Inserting (33) into (32) yields

$$(\mathbf{D}_1 + \mathbf{D}_2\mathbf{T}\mathbf{W}^{-1}\mathbf{Q})\mathbf{A} = \mathbf{Z}_L(\mathbf{D}_3 + \mathbf{D}_4\mathbf{T}\mathbf{W}^{-1}\mathbf{Q})\mathbf{A}.$$

Since this relation should be valid for any $\mathbf{A}$, we finally obtain

$$\mathbf{Z}_L = (\mathbf{D}_1 + \mathbf{D}_2\mathbf{T}\mathbf{W}^{-1}\mathbf{Q})(\mathbf{D}_3 + \mathbf{D}_4\mathbf{T}\mathbf{W}^{-1}\mathbf{Q})^{-1}. \tag{34}$$

In practice, it is advantageous to rescale the two factors of Eq. (34), since otherwise the conditioning number of the resulting system of equations tends to infinity as $L \to -\infty$. The reason for this is that a unit magnitude at $x = 0$ of an evanescent mode would suggest a magnitude that tends to infinity as $x \to -\infty$.

5.1.5. Use of the impedance matrix. Once an impedance matrix has been established, it is used as a boundary condition in the Helmholtz equation by solving Eq. (32) for $\mathbf{B}$. In order to decrease the condition number of the coefficient matrix, it is advantageous to introduce a scaling of the unknowns also in $\mathbf{B}$.

5.1.6. Results. A number of experiments were carried out with the channel of the previous section. For different positions, $x = L$, to the left of the step discontinuity, the IBC $\mathbf{Z}_L$ was computed. $\mathbf{Z}_L$ was then used as a representation of the portion of the channel to the right of $x = L$. The number of modes, N_{BC}, included in the application of the IBC, was much less than the number of modes (160) actually used for the computation of $\mathbf{Z}_L$. The quantities studied were the obtained reflection coefficients of $\mathbf{B}$. All errors have been computed with respect to the reference solution obtained by Romberg extrapolation. Figure 6 shows the relative errors in $\mathbf{B}_0$ for $\omega = 0.5$. The numbers of modes in the left part of the channel was 3, 5, 8 and 13. Figure 7 shows corresponding data for $\mathbf{B}_1$. The horizontal lines show the errors obtained with the coarse discretisations used all through the domain. With $\omega = 3.2$, the acoustical situation is different, since there are now four propagating modes. Figure 8 and 9 show the errors in B_0 and B_1 for this case. Apparently, for $N_{BC} = 3$, the error does not converge to zero as $L \to -\infty$. For $N_{BC} = 4$, the error does converge to zero, although rather slowly. The inclusion of only one evanescent mode improves the situation drastically, which is seen by the curves corresponding to $N_{BC} = 5$.

It should be noted that the accuracy of $\mathbf{Z}_L$ is high because it was created using a great number of modes. In contrast, at $x < x_L$ a much coarser discretisation represented by 3, 5, 8, and 13 modes is used. Still, the accuracy of B_0 is quite good provided that x_L is placed sufficiently far from the discontinuity, for example at $x_L = -0.5$. In terms of the wavelength $\lambda = 2\pi/\omega$, $\omega = 0.5$, $x_L = -0.5$ is only a tiny fraction (approximately 1/25:th) of a wavelength away from the discontinuity at $x = 0$. This implies that the extremely fine discretisation around $x = 0$ can be confined to a narrow strip.

Although only a few elements of $\mathbf{Z}_L$ need be used, a necessary condition is that at least $N_{\text{prop}} \times N_{\text{prop}}$ elements are used. Here, N_{prop} is the number of propagating modes.

Figure 10 shows the relative error in B_0, B_1 and B_2 at $L = -0.5$, as a function of ω. The number of modes considered in $\mathbf{Z}_L$ is three. As expected, the error increases rapidly when ω is higher than the cut-off frequency of B_2. The same investigation for five modes in $\mathbf{Z}_L$ yields the error curves shown in Fig. 11. As the curves show, and in particular in Fig. 11, the errors tend to exhibit maxima near the cut-off frequencies, both for propagating and evanescent modes.

It is imperative to compare the magnitudes of the elements in the impedance matrices for varying frequencies and positions. Figure 12–14 show the results of this study for the upper left 18×18 elements of the matrices. As expected, the

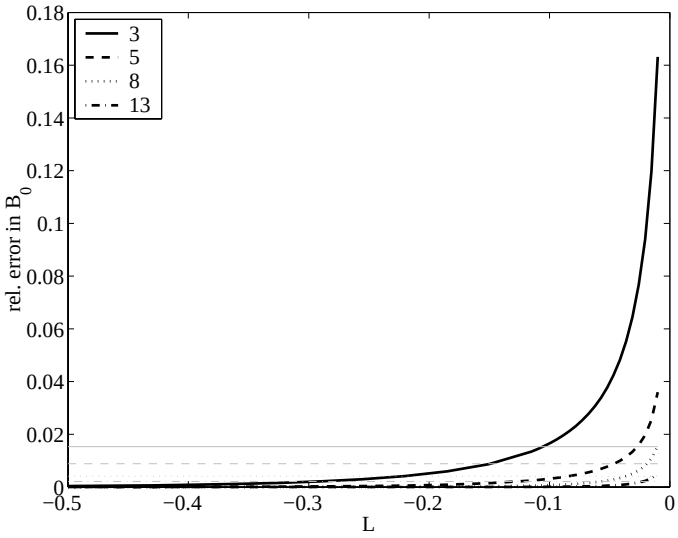

FIG. 6. *Relative error in B_0 as a function of L for different numbers of modes. $\omega = 0.5$.*

modulus of the elements corresponding to evanescent modes decay rapidly away from the upper left corner of the matrix. The decay is slower along the diagonal, however. As the distance to the discontinuity increases, only the diagonal elements and the elements corresponding to propagating modes differ significantly from zero.

5.2. The discrete case. In this section we consider a discretised version of the problem of the previous section. The discretisation is intended to mimic a real problem that is solved using a numerical technique. In this case a second order finite-difference (FD) method is used.

5.2.1. Second order FD solution of the channel problem. The channel is discretised with a structured grid (figure 15), consisting of two sub grids matched at $x = 0$. The grids are denoted G_l and G_r. The grid points are located in such a way that the sound hard boundaries and the junction at $x = 0$ are centred between the nodes. We have

$$x_\ell = (\ell + 1/2)h_x, \quad \ell = \ldots, -2, -1, 0, \quad \text{on } G_l, \tag{35}$$

$$x_\ell = (\ell - 1/2)h_x, \quad \ell = 0, 1, 2, \ldots, \quad \text{on } G_r, \tag{36}$$

$$y_j = jh_y, \quad -N_l \leq j \leq N_l \quad \text{on } G_l, \tag{37}$$

$$y_j = jh_y, \quad -N_r \leq j \leq N_r \quad \text{on } G_r. \tag{38}$$

The Helmholtz equation is solved on the grid using the standard second

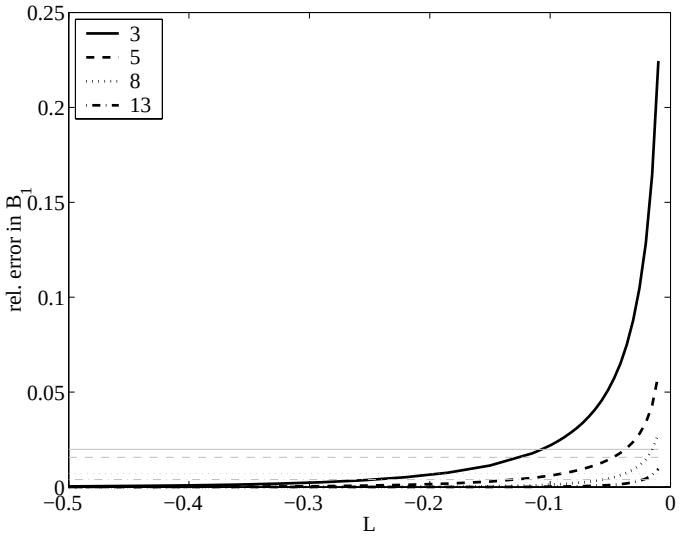

FIG. 7. *Relative error in B_1 as a function of L for different numbers of modes. $\omega = 0.5$.*

order finite-difference scheme

$$\frac{p_{\ell+1,j} - 2p_{\ell,j} + p_{\ell-1,j}}{h_x^2} + \frac{p_{\ell,j+1} - 2p_{\ell,j} + p_{\ell,j-1}}{h_y^2} + k^2 p_{\ell,j} = 0, \tag{39}$$

where

$$p(x_\ell, y_j) \approx p_{\ell,j}.$$

The physical boundary conditions $\partial p/\partial n$ at the wall are implemented using the boundary centred differences

$$p_{\ell,N_l} - p_{\ell,N_l-1} = 0, \quad x_\ell < 0 \tag{40}$$

$$p_{\ell,N_r} - p_{\ell,N_r-1} = 0, \quad x_\ell > 0 \tag{41}$$

$$p_{0,j} - p_{-1,j} = 0, \quad j \leq N_l\,. \tag{42}$$

The general solution to (39) can be found by the method of separation of variables. Using the notations

$$\begin{aligned} d_+^x p_{\ell,j} &= p_{\ell+1,j} - p_{\ell,j} \\ d_-^x p_{\ell,j} &= p_{\ell,j} - p_{\ell-1,j} \\ d_+^y p_{\ell,j} &= p_{\ell,j+1} - p_{\ell,j} \\ d_-^y p_{\ell,j} &= p_{\ell,j} - p_{\ell,j-1} \end{aligned}$$

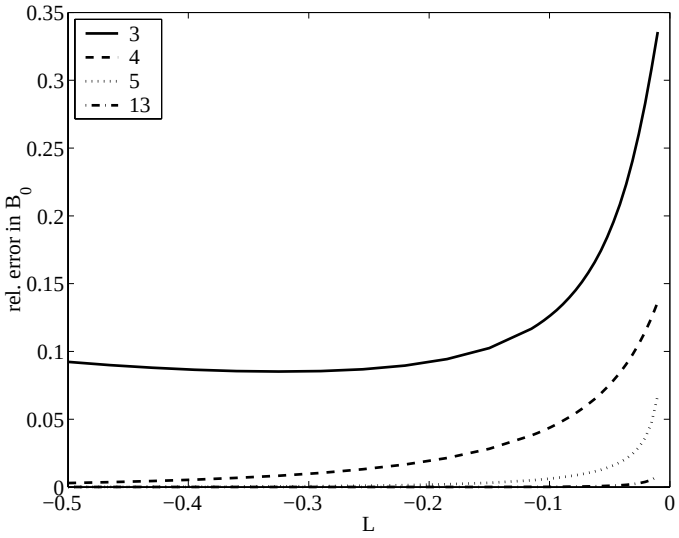

FIG. 8. *Relative error in B_0 as a function of L for different numbers of modes. $\omega = 3.2$.*

and trying the ansatz $p_{\ell,j} = X_\ell Y_j$ yields

$$Y_j \frac{d_+^x d_-^x X_\ell}{h_x^2} + X_\ell \frac{d_+^y d_-^y Y_j}{h_y^2} + k^2 X_\ell Y_j = 0.$$

Dividing by $X_\ell Y_j$ we get

$$\frac{d_+^x d_-^x X_\ell}{X_\ell h_x^2} + \frac{d_+^y d_-^y Y_j}{Y_j h_y^2} + k^2 = 0.$$

Rearranging the terms, and noting that the l.h.s and the r.h.s are functions of j and ℓ only, we can write

$$\frac{d_+^y d_-^y Y_j}{Y_j h_y^2} = -k^2 - \frac{d_+^x d_-^x X_\ell}{X_\ell h_x^2} = -\eta^2,$$

where η is a constant. The j-dependent part,

$$d_+^y d_-^y Y_j + h_y^2 \eta^2 Y_j = 0,$$

of the equation has a solution of the form $Y_j = \exp(i\kappa y_j)$, which gives the following relation for the transversal wave number κ,

$$\cos(\kappa h_y) = 1 - \frac{h_y^2 \eta^2}{2}.$$

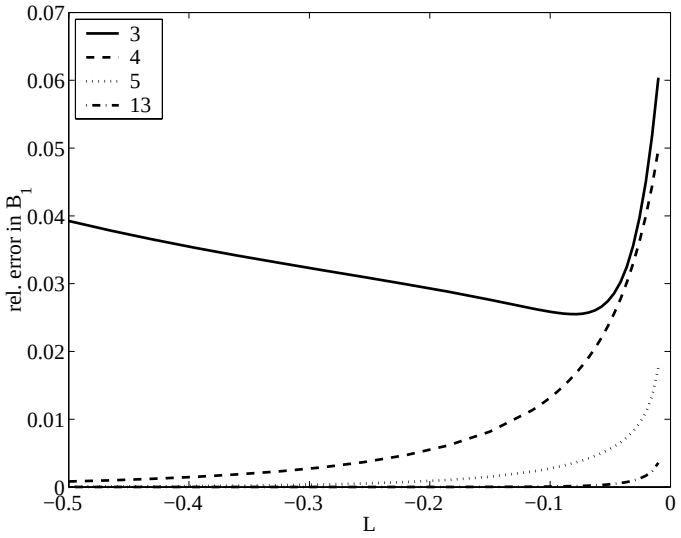

FIG. 9. *Relative error in B_1 as a function of L for different numbers of modes. $\omega = 3.2$.*

The only allowed values of κ are those that comply with the boundary conditions, that is, solutions of the form

$$Y_j = \cos(\kappa y_j) = \frac{n\pi}{r}, \quad r = a, b$$

where

$$\kappa = \frac{n\pi}{(N_{\max} - 1/2)h_y}, \quad N_{\max} = N_l, N_r.$$

Here, $n = 0, 1, 2, \ldots$. For the ℓ-dependent part, we have the equation

$$\frac{d_+^x d_-^x X_\ell}{X_\ell h_x^2} = \eta^2 - k^2$$

or

$$d_+^x d_-^x X_\ell + h_x^2(k^2 - \eta^2)X_j = 0.$$

The solutions to this equation are of the form $X_\ell = \exp(i\xi x_\ell)$, which leaves us with the following relation for the longitudinal wave number ξ,

$$\cos(\xi h_x) = 1 - \frac{h_x^2(k^2 - \eta^2)}{2}.$$

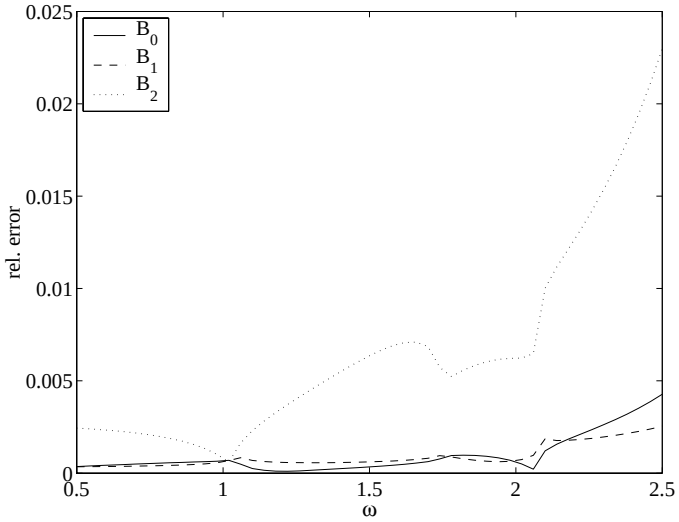

FIG. 10. *Relative error in B_0 through B_2 as a function of ω for three modes. $L = -0.5$.*

The solution to (39) may thus be expressed as

$$p_{l\ell,j} = \sum_{n=0}^{N_l-1} \cos(\kappa_l^{(n)} y_j)(A_n e^{i\xi_l^{(n)} x_l} + B_n e^{-i\xi_l^{(n)} x_l}), \quad x_\ell < 0 \tag{43}$$

$$p_{r\ell,j} = \sum_{n=0}^{N_r-1} \cos(\kappa_r^{(n)} y_j)(C_n e^{i\xi_r^{(n)} x_l} + D_n e^{-i\xi_r^{(n)} x_l}), \quad x_\ell > 0 \tag{44}$$

where $\kappa_l^{(n)}$, $\xi_l^{(n)}$, $\kappa_r^{(n)}$, and $\xi_r^{(n)}$ are the transversal and the longitudinal wave numbers to the left and to the right of $x = 0$, respectively.

The coefficients A_n and D_n are chosen with respect to a prescribed input excitation. B_n and C_n are then chosen in order to satisfy the boundary conditions at $x = 0$. Under the assumption that no waves are excited at $x \to \infty$, we have again that $D_n = 0\,\forall n$. Furthermore, the solution and its normal derivative must be continuous along the internal boundary at $x = 0$. Second order accurate approximations of the continuity conditions yield

$$p_{l0,j} + p_{l-1,j} = p_{r1,j} + p_{r0,j} \qquad -N_r + 1 \le j \le N_r - 1 \tag{45}$$

$$p_{l0,j} - p_{l-1,j} = p_{r1,j} - p_{r0,j} \qquad -N_r + 1 \le j \le N_r - 1 \tag{46}$$

The last condition that must be satisfied is the Neumann condition $\partial p/\partial n = 0$ at the vertical wall at $x = 0$. A second order approximation of this boundary condition is

$$p_{l0,j} - p_{l-1,j} = 0, \quad -N_l \le j \le -N_r \text{ and } N_r \le j \le N_l \tag{47}$$

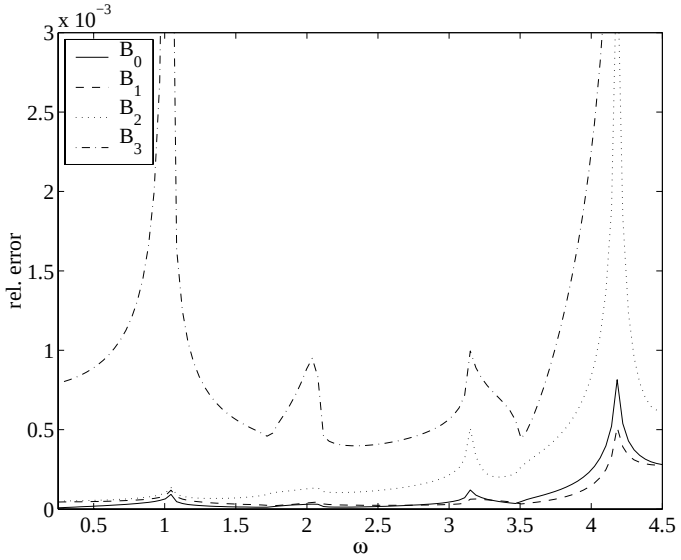

FIG. 11. *Relative error in B_0 through B_3 as a function of ω for five modes. $L = -0.5$.*

Due to symmetry, Eq. (45)–(47) are automatically satisfied for $j < 0$. Putting (43) into the boundary conditions yields the following systems of equations;

$$\sum_{n=0}^{N_l-1} \cos\left(\frac{n\pi}{a} h_y j\right) \left(A_n e^{i\xi_n^l(-\frac{h_x}{2})} + B_n e^{-i\xi_n^l(-\frac{h_x}{2})}\right) = \sum_{n=0}^{N_r-1} C_n \cos\left(\frac{n\pi}{b} h_y j\right) e^{i\xi_n^r(-\frac{h_x}{2})}, \quad j = 0, 1, \ldots N_r - 1 \tag{48a}$$

$$\sum_{n=0}^{N_l-1} \cos\left(\frac{n\pi}{a} h_y j\right) \left(A_n e^{i\xi_n^l(\frac{h_x}{2})} + B_n e^{-i\xi_n^l(\frac{h_x}{2})}\right) = \sum_{n=0}^{N_r-1} C_n \cos\left(\frac{n\pi}{b} h_y j\right) e^{i\xi_n^r(\frac{h_x}{2})}, \quad j = 0, 1, \ldots N_r - 1 \tag{48b}$$

$$\sum_{n=0}^{N_l-1} \cos\left(\frac{n\pi}{a} h_y j\right) \left(A_n e^{i\xi_n^l(-\frac{h_x}{2})} + B_n e^{-i\xi_n^l(-\frac{h_x}{2})}\right) = \sum_{n=0}^{N_r-1} \cos\left(\frac{n\pi}{a} h_y j\right) \left(A_n e^{i\xi_n^l(\frac{h_x}{2})} + B_n e^{-i\xi_n^l(\frac{h_x}{2})}\right), \quad N_r \le j \le N_l \tag{48c}$$

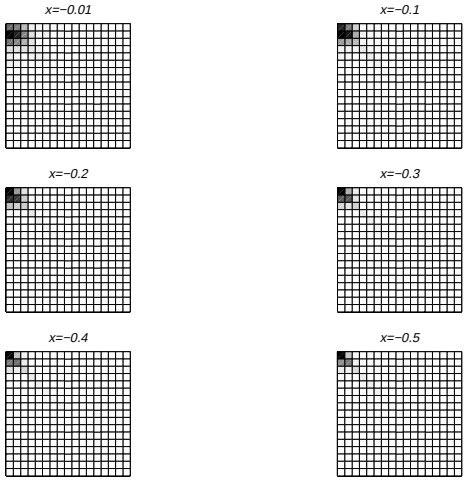

FIG. 12. *Magnitudes of the elements in* $\mathbf{Z}_L$. $\omega = 0.5$.

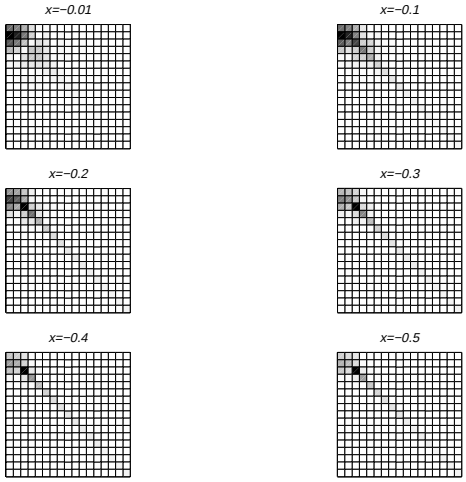

FIG. 13. *Magnitudes of the elements in* $\mathbf{Z}_L$. $\omega = 2.2$.

5.2.2. Computing the discrete impedance matrix. Working with solutions expanded in the vertical eigenmodes, we may write

$$p_{l\ell,j} = \sum_n \tilde{p}_{l\ell,n} \cos(\frac{n\pi}{a} y_j)$$

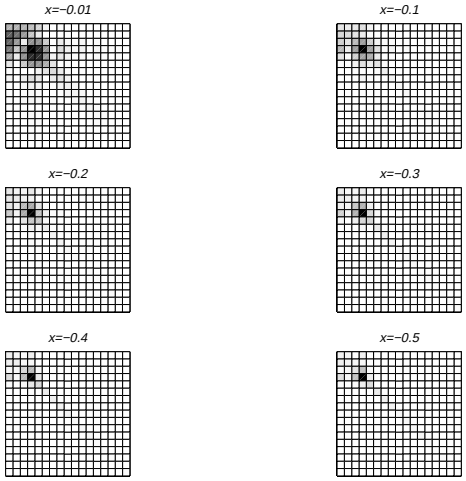

FIG. 14. *Magnitudes of the elements in* $\mathbf{Z}_L$. $\omega = 3.2$.

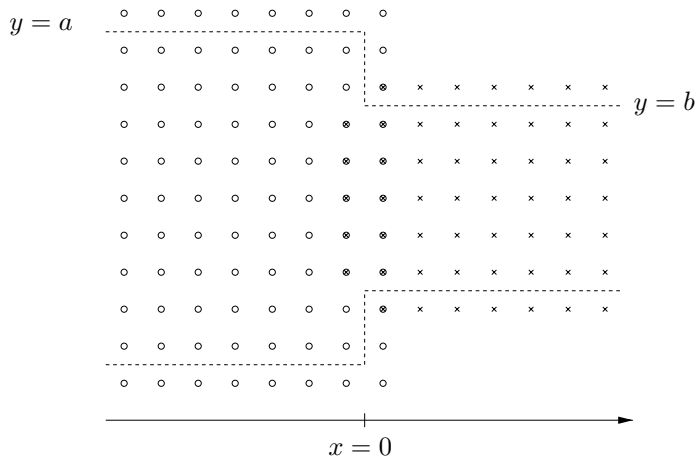

FIG. 15. *A discrete test problem.*

where

$$\tilde{p}_{l_{\ell,n}} = A_n e^{i\xi_l^{(n)} x_\ell} + B_n^{-i\xi_l^{(n)} x_\ell} \tag{49}$$

At a transversal boundary, placed at $x = x_0$, the discrete impedance matrix $\mathbf{Z}_L$ is defined by

$$\frac{1}{2}(\tilde{\mathbf{p}}_0 + \tilde{\mathbf{p}}_{-1}) = \frac{1}{h_x}\mathbf{Z}_H(\tilde{\mathbf{p}}_0 - \tilde{\mathbf{p}}_{-1})\,, \tag{50}$$

where

$$\tilde{\mathbf{p}}_0 = (\tilde{p}_{l\,0,0}, \tilde{p}_{l\,0,1}, \dots \tilde{p}_{l\,0,N_l-1})^T$$

and

$$\tilde{\mathbf{p}}_{-1} = (\tilde{p}_{l\,-1,0}, \tilde{p}_{l\,-1,1}, \dots \tilde{p}_{l\,1,N_l-1})^T.$$

The impedance matrix for the discrete problem can of course be computed along the same lines as in the continuous case. However, in a practical case it is rarely possible to form the counterpart to Eq. (34). This is the situation when, for instance, an iterative solver is used for the solution of the linear system stemming from the discretised Helmholtz equation. The rest of this section illustrates how the impedance can be computed in such a case.

Again restricting the argument to modes symmetric w.r.t $y = 0$, Eq. (50) should be valid for any such $\mathbf{A}$. By prescribing N linearly independent excitation patterns

$$\mathbf{A}^{(k)} = (A_0^{(k)}, A_1^{(k)}, A_2^{(k)}, \dots, A_{N-1}^{(k)})^T, \quad k = 1, 2, \dots, N-1\,,$$

and computing the corresponding responses

$$\mathbf{B}^{(k)} = (B_0^{(k)}, B_1^{(k)}, B_2^{(k)}, \dots, B_{N-1}^{(k)})^T, \quad k = 1, 2, \dots, N-1\,,$$

Eq. (50) can be solved for $\mathbf{Z}_L$. Denoting by $\tilde{\mathbf{p}}_0^{(k)}$ and $\tilde{\mathbf{p}}_{-1}^{(k)}$ the solutions corresponding to $\mathbf{A}^{(k)}$, this is done by inserting

$$\tilde{\mathbf{P}}_0 = [\tilde{\mathbf{p}}_0^{(1)}\, \tilde{\mathbf{p}}_0^{(2)}\, \dots\, \tilde{\mathbf{p}}_0^{(N)}]^T, \quad \tilde{\mathbf{P}}_{-1} = [\tilde{\mathbf{p}}_{-1}^{(1)}\, \tilde{\mathbf{p}}_{-1}^{(2)}\, \dots\, \tilde{\mathbf{p}}_{-1}^{(N)}]^T$$

into Eq. (50), which yields the equation

$$\frac{1}{2}(\tilde{\mathbf{P}}_0 + \tilde{\mathbf{P}}_{-1}) = \frac{1}{h_x}\mathbf{Z}_H(\tilde{\mathbf{P}}_0 - \tilde{\mathbf{P}}_{-1}) \tag{51}$$

for $\mathbf{Z}_L$.

5.2.3. Use of the impedance matrix. The impedance matrix is used in the same way as in the continuous case. The application of the impedance matrix for the discrete model problem has a caveat that does not appear in the continuous version of the problem. Since terms of the type $\exp(\pm i\xi L)$ appear in the reconstruction, a numerical phase error is introduced due to the fact that ξ differs slightly from the physical wave number k. This is a somewhat artificial effect, not relevant when the impedance matrix technique is used in a real case, but makes the interpretation of the errors more difficult. In the results presented here, this phase error has therefore been cancelled by using the physical wavenumbers in the reconstruction phase.

N	3	5	8	13
$\lvert R/B_0 \rvert$	0.088	0.026	0.0094	0.0033

TABLE 6
Ratio of the grid discontinuity reflection R to the physical reflection coefficient B_0.

5.2.4. Results. The same type of study as in the continuous version of the model problem was carried out. The figures 16 and 17 show the results from this investigation. As in the continuous case, the error in B_0 decreases rapidly as the distance between the step discontinuity and the placement of the boundary condition is increased. However, the error does not converge to zero. The reason for this is that although the near field of the corner quickly becomes captured by $\mathbf{Z}_L$, there is a remaining error due to the artificial reflection at the grid resolution discontinuity that is in fact present at $x = L$. This is a well known phenomenon [8] that has to be considered also in a real case. An easy way of seeing how the problem arises is to imagine a situation where Z_L of a half-infinite one dimensional waveguide, discretised with some resolution, is computed. In this case it will be proportional to $c_{numeric}$. When Z_L is used on a grid of different resolution, and hence with a different numerical wave speed, a reflection will occur where there should be none. An estimate of the magnitude of this error in the far field limit can be obtained by comparing the grid discontinuity reflection R to the modulus of B_0. The expression for R is derived in Appendix B. Table 6 shows the ratio $|R/B_0|$ for the experiment at hand. The figures of the table agree well with the levels of the error curves in Fig. 16. The advantage of using a spectral method, like the one of section5.1, is clear.

For B_1, the error actually seem to increase for $N = 3$ and $N = 5$ as $\mathbf{Z}_L$ is moved to the left. The explanation is that these coarse grids are unable to resolve the B_1 mode properly. As N is increased, the error in B_1 starts to decrease as expected, however.

6. Impedance boundary conditions from time-domain simulations. The large scale solution of the Helmholtz equation leads to linear systems of equations that are notoriously problematic to solve iteratively. Iterative solvers, such as the conjugate gradient method or GMRES [4], are efficient provided that a good pre-conditioner for the system of equations can be found. However, it is an inherent property of wave propagation problems that information is propagated and reflected, rather than smeared out or merely transported out of the domain. This makes such pre-conditioners difficult to construct in the general case. If impedance data for a large number of frequencies are of interest, it can be advantageous to instead work in the the time domain, and compute spectral data by Fourier transforming the applicable time series. The approach would then be to test the object, for which the impedance boundary condition is to be computed, for a number of broad band input signals, each of which has

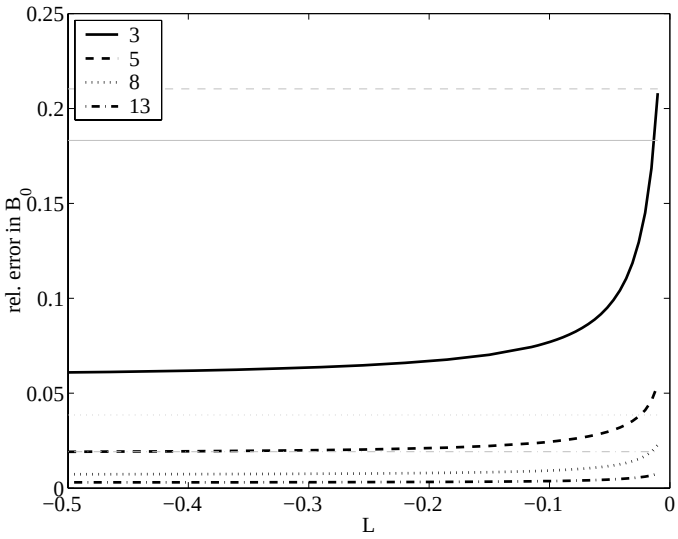

FIG. 16. *Relative error in B_0 as a function of L for different numbers of modes. $\omega = 0.5$.*

a spatial dependence dependence according to the corresponding cross sectional expansion function. In a previous study [15], the author pursued a mono modal version of the approach for the computation of the input impedance of acoustic horns. It is evident that such an approach works best for objects with a short reverberation time, lest the time domain simulations would have to be long before the transient waves decay, something that is essential when computing frequency data from time domain signals.

7. Concluding remarks. This study has treated a simple example which exhibits several essential difficulties that are likely to appear in general. For example, high accuracy of the far-field solution requires a grid refinement in the scattering region. The benefits of using IBC:s in order to connect solutions obtained by different methods and/or different grids have been demonstrated.

The stepped channel used as a model example provides a mathematical problem which needs quite a high number of degrees of freedom in order to achieve accuracy. This is naturally true for the complicated near field in the vicinity of the corner, but also with respect to the simpler far field. This is the case whether a mesh-less mode matching technique or a finite-difference method is used. In reality, the two methods are closely related to each other, and the similarities in the results should come as no surprise.

The importance of selecting matching resolutions on different sides of a discontinuity has been illustrated. A question that is unanswered as of yet is whether this phenomenon appears also for other types of discontinuities, for instance sudden changes of material parameters. If this is the case, great care

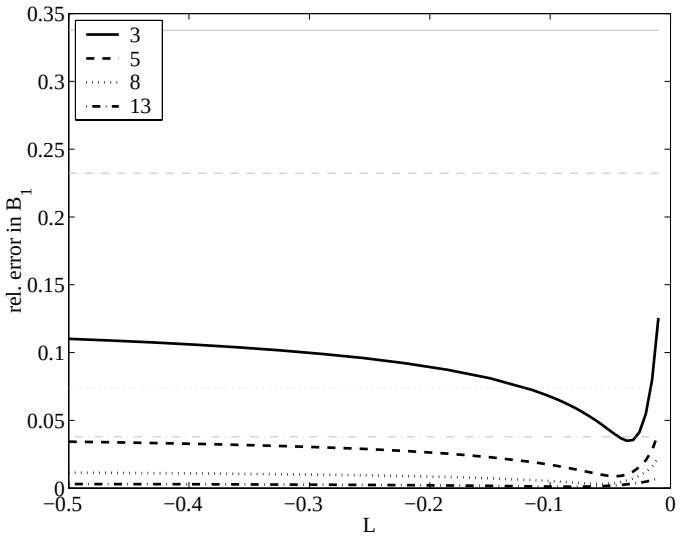

FIG. 17. *Relative error in B_1 as a function of L for different numbers of modes. $\omega = 0.5$.*

must be taken when joining different solution methods, whether it is done by impedance boundary conditions or otherwise. This is a subject to future research.

The impedance boundary condition method can be applied for other numerical methods than the second order finite-difference method presented here. It is also possible that one would wish to use a finite-difference method of higher order than two. This requires some extra attention in the numerical formulation of the boundary condition, but should not present any difficulties in principle. For time domain simulations, the practical difficulties of achieving numerical stability in the time integration can be significant, however.

Acknowledgement. I am indebted to Leif Abrahamsson for his valuable advice and for many fruitful discussions during the course of this work.

APPENDIX A.

Solution to the step discontinuity problem in a cylindrical channel. Let an infinitely long cylindrically symmetric waveguide be defined by

$$\begin{aligned} &r \le a, \quad z \le 0 \\ &r \le b, \quad z > 0, \quad a \ge b, \end{aligned}$$

where $-\infty < z < \infty$. Setting $c = 1$ for simplicity, we look for solutions to the

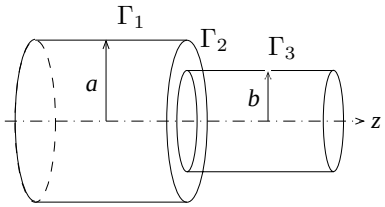

FIG. 18. *Cylindrical waveguide with a step discontinuity.*

cylindrically symmetric Helmholtz equation

$$\begin{aligned} \frac{\partial^2 p}{\partial r^2} + \frac{1}{r}\frac{\partial p}{\partial r} + \omega^2 p &= 0 \\ \frac{\partial p}{\partial n} &= 0 \qquad \text{on } \Gamma_1 \cup \Gamma_2 \cup \Gamma_3, \end{aligned}$$

for waves entering the domain from $z = -\infty$. The solution to this equation can be written as

$$p_l(z,r) = \sum_{n=1}^{\infty} J_0(\eta_{0n} r/a) \left(A_n e^{i\sqrt{\omega^2 - (\eta_{0n}/a)^2}\, z} + B_n e^{-i\sqrt{\omega^2 - (\eta_{0n}/a)^2}\, z} \right), z \le 0$$

$$p_r(z,r) = \sum_{n=1}^{\infty} J_0(\eta_{0n} r/b) \left(C_n e^{i\sqrt{\omega^2 - (\eta_{0n}/b)^2}\, z} + D_n e^{-i\sqrt{\omega^2 - (\eta_{0n}/b)^2}\, z} \right), z > 0,$$

where η_{0n} is the n:th zero of $J_0'(x)$. These solutions satisfy the boundary condition $\partial p/\partial r = 0$ for $z \le 0$ as well as for $z > 0$. Since no waves coming from the right are prescribed, we have $D_n \equiv 0$. The coefficients B_n and C_n now have to be chosen so that $\partial p/\partial z = 0$ for $z = 0^-$. Moreover, both p and $\partial p/\partial z = 0$ should be continuos at $z = 0$ for $r \le b$;

$$p_l(0,r) = p_r(0,r), \quad 0 \le r \le b, \tag{A-1a}$$

$$\frac{\partial p_l(0,r)}{\partial x} = \frac{\partial p_r(0,r)}{\partial z}, \quad 0 \le r \le b. \tag{A-1b}$$

Truncating the expansions to N and M modes, it is possible to formulate a linear system of $M + N$ equations for the unknown coefficients. The coefficient

matrix of this system is obtained by taking the scalar product between Eqn. (A-1a) and $J_0(\eta_{0m}r/b)$ for $m = 1, 2, \ldots, M$,

$$\sum_{n=1}^{N} A_n \int_0^b J_0(\eta_{0n}r/a)J_0(\eta_{0m}r/b)rdr + \sum_{n=1}^{N} B_n \int_0^b J_0(\eta_{0n}r/a)J_0(\eta_{0m}r/b)rdr = \sum_{n=1}^{M} C_n \int_0^b J_0(\eta_{0n}r/b)J_0(\eta_{0m}r/b)rdr, \quad m = 1, 2, \ldots, M \tag{A-2}$$

The choice of the integral kernel r reflects the fact that we are working in a cylindrical symmetry. Similarly, projection of Eqn. (A-1b) on the basis functions yields

$$\sum_{n=1}^{N} i\sqrt{\omega^2 - (\eta_{0n}/a)^2} A_n \int_0^a J_0(\eta_{0n}r/a)J_0(\eta_{0m}r/a)rdr - \sum_{n=1}^{N} i\sqrt{\omega^2 - (\eta_{0n}/a)^2} B_n \int_0^a J_0(\eta_{0n}r/a)J_0(\eta_{0m}r/a)rdr = \sum_{n=1}^{M} i\sqrt{\omega^2 - (\eta_{0n}/b)^2} C_n \int_0^b J_0(\eta_{0n}r/b)J_0(\eta_{0m}r/a)rdr, \quad m = 1, 2, \ldots, N \tag{A-3}$$

The linear system may thus be written

$$\begin{bmatrix} \mathbf{W}^1_{M\times N} & \mathbf{W}^2_{M\times M} \\ \mathbf{W}^3_{N\times N} & \mathbf{W}^4_{N\times M} \end{bmatrix} \begin{bmatrix} \mathbf{B} \\ \mathbf{C} \end{bmatrix} = \begin{bmatrix} \mathbf{Q}^1_{M\times N} \\ \mathbf{Q}^2_{N\times N} \end{bmatrix} \mathbf{A} \tag{A-4}$$

where

$$\begin{aligned} Q^1_{mn} &= \int_0^b J_0(\eta_{0n}r/a)J_0(\eta_{0m}r/b)rdr, \\ Q^2_{mn} &= -\int_0^b J_0(\eta_{0n}r/b)J_0(\eta_{0m}r/b)rdr, \\ Q^3_{mn} &= -i\sqrt{\omega^2 - (\eta_{0n}/a)^2} \int_0^a J_0(\eta_{0n}r/a)J_0(\eta_{0m}r/a)rdr, \\ Q^3_{mn} &= -i\sqrt{\omega^2 - (\eta_{0n}/b)^2} \int_0^b J_0(\eta_{0n}r/b)J_0(\eta_{0m}r/a)rdr, \end{aligned}$$

and

$$\mathbf{Q}^1 = -\mathbf{W}^1, \quad \mathbf{Q}^2 = \mathbf{W}^3 .$$

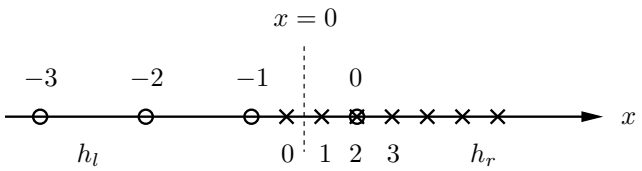

FIG. 19. *One-dimensional discontinuous grid with the numbering of the grid points indicated.*

APPENDIX B.

Reflection at a grid discontinuity. Consider the one-dimensional grid defined by Fig. 19. It consists of two half-infinite discretisations of the x-axis with unequal step sizes h_l and h_r. $x = 0$ is centered between two grid points from the respective sub-discretisations. On this grid, the Helmholtz equation $\partial^2 p/\partial x^2 + k^2 p = 0$ is solved using the standard second order finite difference method. For a right travelling incoming wave of unit magnitude, the solution can be written

$$p_{l\ell} = e^{i\xi_l x_{l\ell}} + Re^{-i\xi_l x_{l\ell}}, \tag{B-1a}$$

$$p_{r\ell} = Te^{i\xi_r x_{r\ell}}, \tag{B-1b}$$

to the left and to the right of $x = 0$. Here $x_{l\ell} = (\ell+1/2)h_l$ and $x_{r\ell} = (\ell-1/2)h_r$. R and T can be identified as the reflection and the transmission coefficients for a wave meeting the discontinuity from the left. On a grid with step size h, the numerical wavenumber ξ for the scheme at hand is related to the physical wavenumber through the relation

$$\cos(\xi h) = 1 - \frac{h^2 k^2}{2}. \tag{B-2}$$

The discrete continuity conditions at $x = 0$ is

$$p_{l\,-1} + p_{l0} = p_{r0} + p_{r1} \tag{B-3a}$$

$$\frac{1}{h_l}(p_{l0} - p_{l\,-1}) = \frac{1}{h_r}(p_{r1} - p_{l0}). \tag{B-3b}$$

Inserting Eqn. (B-1) into Eqn. (B-3) yields the system of equations

$$\begin{aligned} e^{-i\xi_l h_l/2} + Re^{i\xi_l h_l/2} + e^{i\xi_l h_l/2} + Re^{-i\xi_l h_l/2} = \\ Te^{-i\xi_r h_r/2} + Te^{i\xi_r h_r/2}, \\ \frac{1}{h_l}\left(e^{i\xi_l h_l/2} + Re^{-i\xi_l h_l/2} - e^{-i\xi_l h_l/2} - Re^{i\xi_l h_l/2}\right) = \\ \frac{1}{h_r}\left(Te^{i\xi_r h_r/2} - Te^{-i\xi_r h_r/2}\right), \end{aligned}$$

or

$$\begin{bmatrix} \cos(\xi_r h_r/2) & -\cos(\xi_r h_r/2) \\ -i\sin(\xi_l h_l/2)/h_l & -i\sin(\xi_r h_r/2)/h_r \end{bmatrix} \begin{bmatrix} R \\ T \end{bmatrix} = \begin{bmatrix} -\cos(\xi_r h_r/2) \\ -i\sin(\xi_l h_l/2)/h_l \end{bmatrix}$$

with the solution for R

$$R = \frac{\sin(\xi_l h_l/2)\cos(\xi_r h_r/2)h_r - \cos(\xi_l h_l/2)\sin(\xi_r h_r/2)h_l}{\sin(\xi_l h_l/2)\cos(\xi_r h_r/2)h_r + \cos(\xi_l h_l/2)\sin(\xi_r h_r/2)h_l}.$$

where ξ_l and ξ_r are solutions to Eqn. (B-2) for $h = h_l$ and $h = h_r$.

REFERENCES

[1] A. Craggs. The application of the transfer matrix and matrix condensation methods with finite elements to duct acoustics. *J. Sound and Vibration*, 132:241–254, 1989.

[2] K. Eriksson, D. Estep, P. Hansbo, and C. Johnson. Introduction to adaptive methods for differential equations. *Acta Numerica*, pages 105–158, 1995.

[3] D. Gottlieb and S. A. Orszag. *Numerical Analysis of Spectral Methods: Theory and Application*. SIAM, Philadelphia, 1977.

[4] A. Greenbaum. *Iterative methods for solving linear systems*. SIAM, Philadelphia, 1997.

[5] C. Johnson. *Numerical solution of partial differential equations by the finite element method*. Studentlitteratur, Lund, 1987.

[6] J. Kergomard. Calculation of discontinuities in waveguides using mode-matching method: an alternative to the scattering matrix approach. *J. Acoustique*, 75:111–138, 1991.

[7] L. E. Kinsler, A. R. Frey, A. B. Coppens, and J. V. Sanders. *Fundamentals of acoustics*. John Wiley & Sons, New York, 1982.

[8] H. Kreiss and J. Oliger. Methods for the approximate solution of time dependent problems. Technical Report 10, WMO/ICSU Joint Organising Committee, GARP Publications Series, 1973.

[9] J. Lighthill. *Waves in fluids*. Cambridge University Press, Cambridge, 1978.

[10] I.-T. Lu, H. K. Jung, and C. M. Tsai. Hybrid combinations of global and local operators for solving helmholtz and poisson equations. *J. Comp. Phys.*, 103:390–401, 1992.

[11] R. Mittra, T. Itoh, and T. Li. Analytical and numerical studies of the relative convergence phenomenon arising in the solution of an integral equation by the moment method. *IEEE Transactions on micriwave theory and techniques*, MTT-20(2):96–104, 1972.

[12] R. T. Muehleisen. *Reflection, radiation, and coupling of higher order modes at discontinuities in finite length rigid walled rectangular ducts*. PhD thesis, The Pennsylvania State Univesity, Pennsylvania, 1996.

[13] R. T. Muehleisen and D. C. Swanson. Modal coupling in acoustic waveguides: planar discontinuities. *Applied Acoustics*, 63:1375–1392, 2002.

[14] B. Nilsson. Acoustic transmission in curved ducts with varying cross-section. *Proc. R. Soc. London*, 458:1555–1574, 2002.

[15] D. Noreland. A Numerical Method for Acoustic Waves in Horns. *Acta Acustica united with Acustica*, 88:576–586, 2002.

[16] S. V. Tsynkov. Numerical solution of problems on unbounded domains: A review. *Appl. Numer. Math.*, 27:465–532, 1998.